PHYSICAL REVIEW B **90**, 214519 (2014)

Electronic structure reconstruction of $Ca_{1-x}Pr_xFe_2As_2$ in the collapsed tetragonal phase

D. F. Xu,[1] D. W. Shen,[2,*] J. Jiang,[1] Z. R. Ye,[1] X. Liu,[1] X. H. Niu,[1] H. C. Xu,[1] Y. J. Yan,[1] T. Zhang,[1] B. P. Xie,[1] and D. L. Feng[1,†]

[1]*State Key Laboratory of Surface Physics, Department of Physics, and Laboratory of Advanced Materials, Fudan University, Shanghai 200433, People's Republic of China*

[2]*State Key Laboratory of Functional Materials for Informatics, Shanghai Institute of Microsystem and Information Technology (SIMIT), Chinese Academy of Sciences, Shanghai 200050, People's Republic of China*

(Received 27 October 2014; revised manuscript received 7 December 2014; published 22 December 2014)

We report the electronic structure reconstruction of $Ca_{1-x}Pr_xFe_2As_2$ in the low temperature collapsed tetragonal (CT) phase observed by angle-resolved photoemission spectroscopy. Different from $Ca(Fe_{1-x}Rh_x)_2As_2$ and the annealed $CaFe_2As_2$ where all hole Fermi surfaces are absent in their CT phases, the cylindrical hole Fermi surface still persists in the CT phase of $Ca_{1-x}Pr_xFe_2As_2$. Furthermore, we found at least three well separated electronlike bands around the zone corner in the CT phase of $Ca_{1-x}Pr_xFe_2As_2$, which are more dispersive than the electronlike bands in the high temperature tetragonal phase. Based on these observations, we propose that the weakening of correlations (as indicated by the reduced effective mass), rather than the lack of Fermi surface nesting, might be responsible for the absence of magnetic ordering and superconductivity in the CT phase.

DOI: 10.1103/PhysRevB.90.214519 PACS number(s): 74.25.Jb, 74.70.−b, 79.60.−i, 71.20.−b

I. INTRODUCTION

The interplay of magnetism, lattice, and superconductivity is an important issue in iron-based superconductors. Typically, the ground state of iron pnictides is a magnetically ordered collinear-antiferromagnetic (CAF) state [1,2]. Carrier doping or the application of hydrostatic pressure can gradually suppress the CAF order and then lead to the emergence of a superconducting dome in the phase diagram [3–5]. On the other hand, under 0.35 GPa hydrostatic pressure, $CaFe_2As_2$ was found to undergo a remarkable structural transition to a collapsed tetragonal (CT) phase at low temperatures [6–8]. Intriguingly, this CT phase, characterized by the shrinkage in the c direction by approximately 10% without breaking the symmetry, is nonmagnetic and nonsuperconducting. As shown by calculations, neutron scattering and x-ray emission spectroscopy, Fe local moments are absent in the CT phase [8–12]. Therefore, it provides a unique platform for studying a nonsuperconducting iron-pnictide system without Fe local moments. From a different perspective, this would facilitate the understanding of the electronic structure which is relevant to superconductivity and local moments in the superconducting iron pnictides.

Angle-resolved photoemission spectroscopy (ARPES) is one of the most direct methods of studying the electronic structure of solids. However, reports on the CT phase had been limited by the necessity of external pressure. Early on, since the nonmagnetic phosphide $CaFe_2P_2$ is a close structural analog of $CaFe_2As_2$ in the CT phase, its electronic structure is considered to somewhat reflect the electronic behavior of the CT phase [13]. The de Haas–van Alphen study showed that the Fermi surface of $CaFe_2P_2$ is highly three-dimensional and the hole pocket only exists around the Z point of the Brillouin zone, which is very different from the electronic structure of an iron-pnictide superconductor. Recently, the CT phase was found to be stabilized under ambient pressure through introducing chemical pressure by specific dopants or thermal treatment [14,15]. Subsequent ARPES experiments on $Ca(Fe_{1-x}Rh_x)_2As_2$ [16] and the annealed $CaFe_2As_2$ [17,18] have revealed significant differences in the electronic structure between the high temperature tetragonal (HT) phase and the CT phase. The predicted vanishment of the hole pocket at the zone center [9,19,20] has been confirmed in both cases. The Fermi surface nesting between electron and hole Fermi surfaces thus vanishes, which was argued to be responsible for the absence of magnetic fluctuation and superconductivity in the CT phase [16,17].

$Ca_{1-x}Pr_xFe_2As_2$ is one of the several iron pnictides that undergo the CT transition under ambient pressure upon cooling [8,15,21–25]. However, little is known about its electronic structure to date. To examine the common properties of the band reconstruction across the transition, it is worthwhile to study the low-lying electronic structure of $Ca_{1-x}Pr_xFe_2As_2$, which might provide clues to understand the interplay of magnetism, lattice, and superconductivity in iron-based superconductors.

In this paper, we report a detailed ARPES study on $Ca_{1-x}Pr_xFe_2As_2$ single crystals. The electronic structure in the HT phase resembles that of the parent compound $CaFe_2As_2$ in its paramagnetic state. Across the CT transition, bands around the zone center shift towards different directions. However, the cylindrical hole Fermi surface can still be observed in its CT phase. This is different from the CT phases of $Ca(Fe_{1-x}Rh_x)_2As_2$ and the annealed $CaFe_2As_2$, in which all hole Fermi surfaces are absent. At least three well separated electronlike bands can be resolved around the zone corner in the CT phase. This contradiction indicates that the absence of magnetic ordering and superconductivity in the CT phase is not correlated with the presence or absence of hole pockets. Our polarization dependence data show strong orbital mixing for the bands in the CT phase. Illustrated by the detailed temperature dependence data, band reconstruction occurs abruptly across the transition, and the hysteresis of reconstruction in the temperature cycle further confirms its

---

[*] dwshen@mail.sim.ac.cn

[†] dlfeng@fudan.edu.cn

first order nature. By comparing the effective masses of the bands in these two phases, we propose that the suppression of electronic correlation, rather than the lack of Fermi surface nesting, might be responsible for the absence of magnetic fluctuation and superconductivity in the CT phase [26]. Our results indicate that the electronic structure of the CT phase of $Ca_{1-x}Pr_xFe_2As_2$ is rather different from those of other known CT compounds, and thus might help facilitate a more comprehensive understanding of the CT phase.

II. SAMPLE PROPERTIES AND EXPERIMENTAL SETUP

High quality $Ca_{1-x}Pr_xFe_2As_2$ single crystals were synthesized by the FeAs self-flux method as described elsewhere [27]. The typical dimension of our samples is $3 \times 2.5 \times 0.1$ mm^3 as shown by the inset in Fig. 1(a). The narrow peak in the x-ray diffraction pattern [Fig. 1(a)] guarantees these samples to be free of foreign phases. The hysteretic drops in magnetic susceptibility [Fig. 1(c)] correspond to the CT structural transition [15,23]. Also, it has been reported that there exist a sudden change and hysteresis of the Hall coefficient around the transition temperature [15]. Both changes imply the drastic change of the electronic structure across the CT transition therein. However, no evident anomaly can be found in the resistivity [Fig. 1(f)], which is consistent with many previous transport works [15,21,22]. Moreover, two drops in resistivity near 20 and 40 K indicate the possible existence of two superconducting phases [21,25], but they are surprisingly doping independent [28]. Though the origin remains unclear, it has been indicated that this superconductivity is neither the bulk nor the intrinsic properties of $Ca_{1-x}Pr_xFe_2As_2$ [15,23,25,28]. We have studied samples with two compositions ($x = 0.1$ and 0.15). The electron probe microanalysis gives an actual chemical composition of Ca:Pr:Fe:As = 0.967:0.152:2.000:2.010 for $x = 0.1$, and 0.931:0.231:2.000:2.024 for $x = 0.15$ samples (normalized to the stoichiometric value of Fe), respectively. Besides slightly changing the chemical potential (<10 meV), we found that the concentration of praseodymium barely affects the electronic structure. Thus, we only present representative data in each section for simplicity.

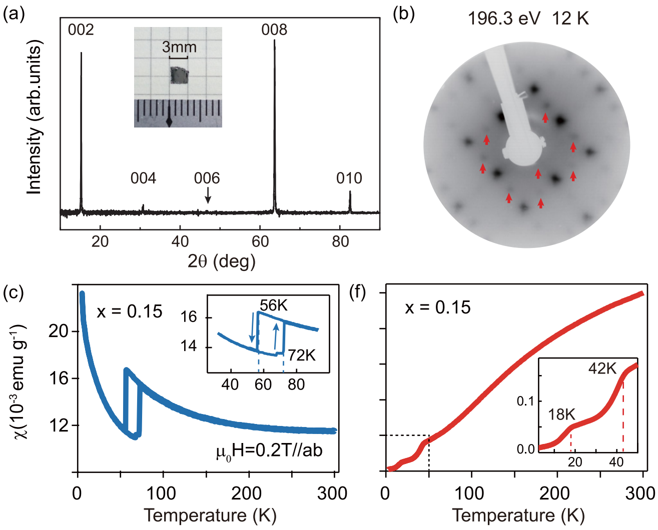

FIG. 1. (Color online) The crystallographic and transport properties of $Ca_{1-x}Pr_xFe_2As_2$. (a) The x-ray diffraction pattern for our single crystal. The inset is a photograph of a typical sample. (b) The low-energy electron diffraction pattern taken in the CT phase at 15 K, showing 1×2 and 2×1 surface reconstructions marked by red arrows. (c) dc susceptibility as a function of temperature under a magnetic field of 0.2 T. Data around the hysteretic drops are magnified in the insets, which correspond to the CT transition. (d) The temperature dependence of the electrical resistivity. Data at low temperatures are magnified in the insets.

ARPES measurements were performed at (i) Beamline 5-4 of Stanford Synchrotron Radiation Lightsource (SSRL), (ii) the SIS beamline of the Swiss Light Source (SLS), and (iii) an in-house system equipped with a SPECS UVLS helium discharge lamp. VG-Scienta R4000 electron analyzers are equipped in all setups. The angular resolution was 0.3° and the overall energy resolution was better than 15 meV. Samples were cleaved *in situ* and measured under ultrahigh vacuum better than 5×10^{-11} torr. The cleaved sample surface exhibits 1×2 and 2×1 reconstructions [Fig. 1(b)], which are frequently observed in cleaved AFe_2As_2 compounds [24,29,30]. A recent scanning tunneling microscopy study on $Ca_{1-x}Pr_xFe_2As_2$ identified the 1×2 and 2×1 surface as a half-Ca termination [24], which preserves the charge neutrality. This is a must for the surface to be representative of the bulk.

III. EXPERIMENTAL RESULTS

A. Band structures in the HT phase and the CT phase

The electronic structure of $Ca_{1-x}Pr_xFe_2As_2$ in the HT phase is presented in Fig. 2. The Fermi surface consists of a large square hole pocket around the zone center and two concentric elliptical electron pockets at the zone corner as illustrated in Fig. 2(a). The photoemission intensity plot and its second derivative with respect to energy along cut 1 [indicated in Fig. 2(a)] are shown in Figs. 2(b) and 2(c), respectively. At the zone center, two bands (assigned as β and ζ) can be identified by tracking the peaks in the corresponding energy distribution curves (EDCs) in Fig. 2(d). The β band crosses the Fermi level (E_F) while the band top of ζ is located at about −100 meV. In this photon energy, the holelike band α is hard to resolve directly due to the overwhelming intensity of the broad β band. At the zone corner along cut 2 [Fig. 2(e)], one broad electronlike feature can be resolved. This feature should be contributed by two electronlike bands (assigned as δ and η), which could be better distinguished in other k_z planes and would be shown later. Overall, the band structure of $Ca_{1-x}Pr_xFe_2As_2$ in the HT phase resembles that of $Ca_2Fe_2As_2$ in the paramagnetic state reported by previous ARPES experiments [31,32].

The Fermi surface topology and band structure of $Ca_{1-x}Pr_xFe_2As_2$ change dramatically in the CT phase as shown in Fig. 3. The reconstructed Fermi surface consists of a smaller square hole pocket around the zone center and several rather complicated electron pockets at the zone corner [Fig. 3(a)]. The disconnection of the Fermi surface contours might be due to the matrix element effects. The photoemission intensity plot and its second derivative with respect to energy

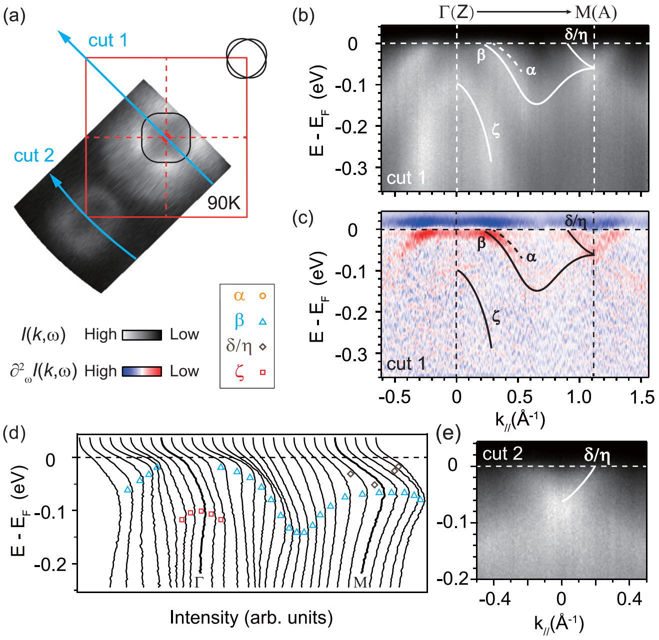

FIG. 2. (Color online) Electronic structure of $Ca_{1-x}Pr_xFe_2As_2$ in the HT phase. (a) The photoemission intensity map integrated over $[E_F - 5\text{ meV}, E_F + 5\text{ meV}]$. Solid black lines represent the Fermi surface contours. Cut directions are indicated by blue arrows. (b), (c) The photoemission intensity plot and its second derivative with respect to energy along cut 1. (d) The selected EDCs for data in panel (b). (e) The photoemission intensity plot along cut 2. Solid lines in panels (b), (c), and (e) are a guide for the eyes for band dispersions. Data were taken with randomly polarized 21.2 eV photons at 90 K.

along cut 1 are shown in Figs. 3(b) and 3(c), respectively. Three bands around the zone center (assigned as $\alpha_{\rm CT}$, $\beta_{\rm CT}$, and $\zeta_{\rm CT}$) could be resolved. From the EDCs shown in Fig. 3(d), $\alpha_{\rm CT}$ crosses Fermi level while the band top of $\beta_{\rm CT}$ is located at -10 meV. The fast dispersing $\zeta_{\rm CT}$ may originate from ζ, and its band top moves from -100 meV to about -70 meV. Around the zone corner, the photoemission intensity plot and its second derivative with respect to energy along cut 2 are plotted in Figs. 3(e) and 3(f), respectively. Eight Fermi crossings can be clearly distinguished by the fitting of the momentum distribution curves (MDCs) near E_F as indicated in Fig. 3(g), six of which belong to three electronlike bands (assigned as $\delta_{\rm CT}$, $\eta_{\rm CT}$, and $\kappa_{\rm CT}$), which can be further confirmed by tracking the peaks in MDCs below E_F in Fig. 3(h). However, it is hard to determine whether the band with the largest crossings (assigned as $\sigma_{\rm CT}$) is a holelike band around the zone center or an electronlike band around the zone corner. Moreover, faint intensity is detected around the X point (not shown here). This additional intensity is consistent with the folding of bands induced from the 1×2 and 2×1 reconstructions at the surface [30]. The main feature of the electronic structure of the CT phase of $Ca_{1-x}Pr_xFe_2As_2$ is that bands tend to be more dispersive in general. For example, around the zone corner, the Fermi velocity of $\delta_{\rm CT}$, $\eta_{\rm CT}$, and $\sigma_{\rm CT}$ is larger than that of δ (η) in the HT phase. This indicates that the electronic correlations are suppressed in the CT phase.

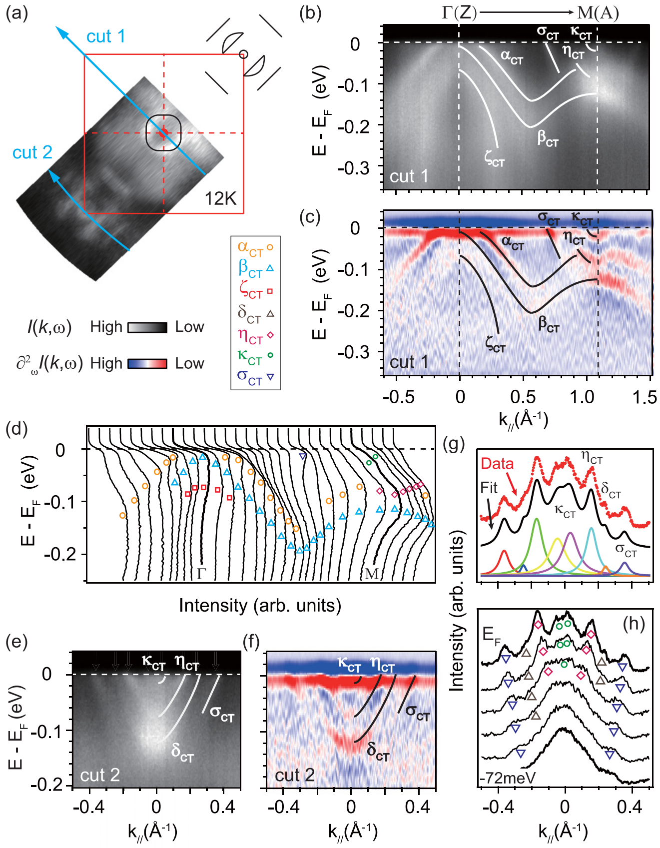

FIG. 3. (Color online) Electronic structure of $Ca_{1-x}Pr_xFe_2As_2$ in the CT phase. (a) The photoemission intensity map integrated over $(E_F - 5\text{ meV}, E_F + 5\text{ meV})$. Solid black lines represent the Fermi surface contours. Cut directions are indicated by blue arrows. (b), (c) The photoemission intensity plot and its second derivative with respect to energy along cut 1. (d) The selected EDCs for data in panel (b). (e), (f) The photoemission intensity plot and its second derivative with respect to energy along cut 2. (g) The MDC integrated over $(E_F - 6\text{ meV}, E_F + 6\text{ meV})$ fitted by eight Lorentzian peaks. (h) The corresponding MDCs near E_F in panel (e). Solid lines in panels (b), (c), (e), and (f) are a guide for the eyes for band dispersions. Data were taken with randomly polarized 21.2 eV photons at 12 K.

All the above data were taken with 21.2 eV photons. However, the sizable contraction of lattice parameter c across the transition can result in the expansion of the reciprocal lattice along the k_z direction, which means that the data taken in the HT and CT phase lie in different k_z planes. If the electronic structure of $Ca_{1-x}Pr_xFe_2As_2$ is highly three-dimensional, it is probable that the differences observed above are merely related to k_z dispersions. To rule out this possibility, photon-energy-dependent ARPES experiments were performed. Our data cover more than half of the Brillouin zone along k_z direction. Considering the periodicity of the band dispersions along the k_z direction, we use an inner potential of 16 eV to determine the corresponding high-symmetry points.

The photon-energy dependencies of the bands in the HT phase are presented in Fig. 4. At the zone center, two representative photoemission intensity plots taken with different photon energies are compared in Figs. 4(b) and 4(c). The intensities of α and β show anticorrelation with each other. While β is

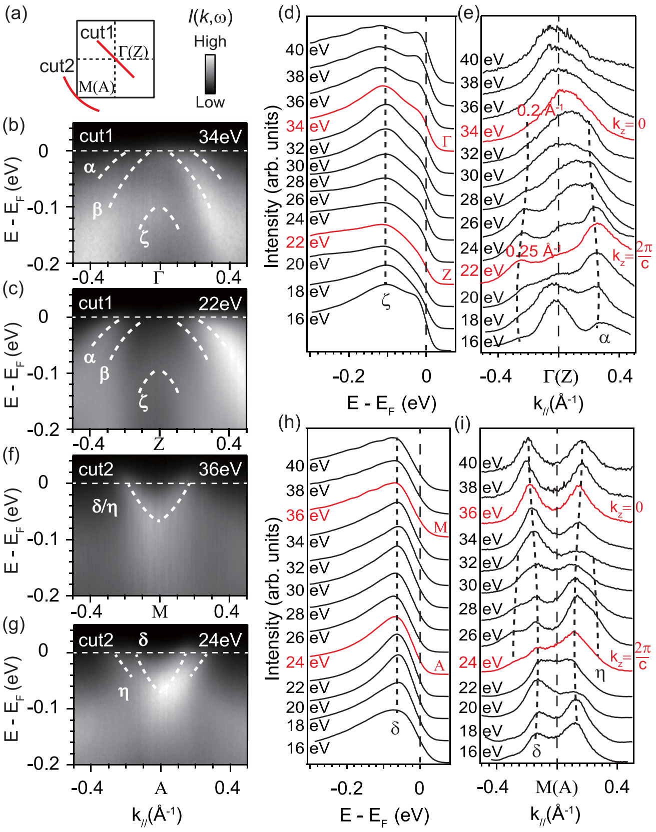

FIG. 4. (Color online) Photon-energy dependence of bands of $Ca_{1-x}Pr_xFe_2As_2$ in the HT phase at 115 K. (a) Indication of cut directions in the projected two-dimensional Brillouin zone. (b), (c) The photoemission intensity plots along cut 1 taken with 34 and 22 eV photons, respectively. (d) The photon-energy dependence of the EDCs at $\Gamma(Z)$. (e) The photon-energy dependence of the MDCs at E_F along cut 1. The Fermi crossings of α in the corresponding high-symmetry planes are shown. (f), (g) The photoemission intensity plots along cut 2 taken with 36 and 24 eV photons, respectively. (h) The photon-energy dependence of the EDCs at $M(A)$. (e) The photon-energy dependence of the MDCs at E_F along cut 2. Dashed lines in panels (b), (c), (f), and (g) are a guide for the eyes for band dispersions.

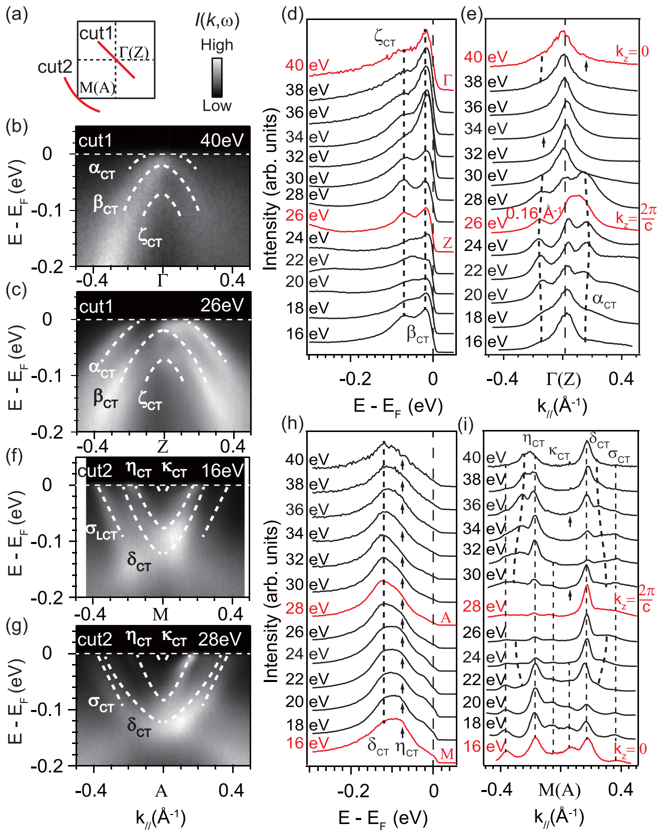

FIG. 5. (Color online) Photon-energy dependence of bands of $Ca_{1-x}Pr_xFe_2As_2$ in the CT phase at 6 K. (a) Indication of cut directions in the projected two-dimensional Brillouin zone. (b), (c) The photoemission intensity plots along cut 1 taken with 40 and 26 eV photons, respectively. (d) The photon-energy dependence of the EDCs at $\Gamma(Z)$. (e) The photon-energy dependence of the MDCs at E_F along cut 1. The Fermi crossings of α_{CT} in the corresponding high-symmetry plane is shown. (f), (g) The photoemission intensity plots along cut 2 taken with 16 and 28 eV photons, respectively. (h) The photon-energy dependence of the EDCs at $M(A)$. (e) The photon-energy dependence of the MDCs at E_F along cut 2. Dashed lines in in panels (b), (c), (f), and (g) are a guide for the eyes for band dispersions.

at its strongest around the Γ point [Fig. 4(b)], α is mostly enhanced around the Z point [Fig. 4(c)]. However, there is rather little variation in the band dispersions. For instance, the band tops of ζ show negligible k_z dependence as illustrated in Fig. 4(d). As for α, the MDCs at E_F in Fig. 4(e) show slight changes in the Fermi crossings upon variation in photon energy, indicative of its moderate k_z dependence. The intensity of α becomes faint around the Γ point, which is probably due to the differences in photoemission matrix element. Around the zone corner [Figs. 4(f)–4(i)], the broad electronlike band splits into two bands at specific photon energies as illustrated in Figs. 4(g) and 4(i). The broad peaks in EDCs around −70 meV correspond to the band bottom of δ, and their positions do not change with photon energies.

In the CT phase (Fig. 5), the representative photoemission intensity plots taken with different photon energies are shown in Figs. 5(b), 5(c), 5(f), and 5(g). As illustrated in Figs. 5(b)–5(e), the intensities of α_{CT}, β_{CT}, and ζ_{CT} behave almost the same as those of α, β, and ζ in the HT phase, except their band tops are located at different binding energies, as mentioned above. At the zone corner [Figs. 5(f)–5(i)], the band bottoms of δ_{CT} and η_{CT} do not vary with photon energies [Fig. 5(h)]. In Fig. 5(i), the peak positions of η_{CT} and σ_{CT} in MDCs at E_F show negligible k_z dependence, while the Fermi crossing of δ_{CT} varies slightly, indicating its moderate k_z dispersion.

The observed photon-energy dependency indicates the electronic structure of $Ca_{1-x}Pr_xFe_2As_2$ to be quasi-two-dimensional. To avoid the ambiguity brought by k_z dispersions, we qualitatively analyze the reconstruction of α in two phases in the same k_z plane [Figs. 4(e) and 5(e)]. In the $2\pi/c$ plane, the Fermi crossings of α change from 0.25 Å^{-1} to 0.16 Å^{-1} across the transition. Here we note in Fig. 4(e), even the largest difference caused by k_z is merely 0.05 Å^{-1}. This clearly points out that the difference of electronic structure is caused by the structural transition. Moreover, the band tops of ζ, ζ_{CT} and the band bottoms of δ, δ_{CT} show negligible k_z dependence. These may be exploited to study the temperature dependence of the reconstruction in data taken with the same photon energy.

B. Polarization dependence

To further understand the electronic structure of $\mathrm{Ca}_{1-x}\mathrm{Pr}_x\mathrm{Fe}_2\mathrm{As}_2$, polarization-dependent measurements were conducted at SLS to identify the orbital characters of band structure. Figure 6(a) illustrates two types of experimental setup with linearly polarized photons. The incident beam and the sample surface normal define a mirror plane. For the p (or s) experimental geometry, the electric field direction ($\hat{\varepsilon}$) of the incident photons is parallel (or perpendicular) to the mirror plane. The matrix element of the photoemission process can be described by

$$\left|M_{f,i}^{k}\right|^2 \propto \left|\langle\phi_f^{\mathbf{k}}|\hat{\varepsilon}\cdot\mathbf{r}|\phi_i^{\mathbf{k}}\rangle\right|^2,$$

where $\phi_i^{\mathbf{k}}$ and $\phi_f^{\mathbf{k}}$ are the initial- and final-state wave functions. In our experimental setup, the momentum of the final-state photoelectron is in the mirror plane and $\phi_f^{\mathbf{k}}$ can be approximated by a plane wave. Therefore, $\phi_f^{\mathbf{k}}$ is always even with respect to the mirror plane. Thus considering the spacial symmetry of the Fe 3d orbitals [Fig. 6(c)], when the analyzer slit is along the high-symmetry directions, the photoemission intensity of a specific even (or odd) component of a band is only detectable with the p (or s) polarized photons [33,34]. For example, with respect to the mirror plane, the even orbitals (d_{xz}, d_{z^2}, and $d_{x^2\text{-}y^2}$) and the odd orbitals (d_{xy} and d_{yz}) could be only observed in the p and s geometries, respectively.

In the HT phase [Figs. 6(d1) and 6(e1)], α (β and δ/η) can be distinguished in the p (s) geometry, indicating that their orbital characters should be even (odd). According to previous knowledge on iron pnictides [33,34], we can ascribe α to the d_{xz} orbital, β to the d_{yz} orbital, while $\delta(\eta)$ can be ascribed to the d_{xy} orbital along these momentum cuts. The intensity of the ζ band is weak in both p and s geometry, and thus it is hard to determine its orbital character. In the CT phase [Figs. 6(d2) and 6(e2)], α_{CT}, β_{CT}, ζ_{CT}, and κ_{CT} show up in both geometries, suggesting that they are mixtures of odd and even orbitals. The σ_{CT} band can be resolved in the p geometry, so it should be made of even orbitals, while δ_{CT} and η_{CT} are present in the s geometry, indicating that their orbital characters should be odd.

The orbital characters of the band structure are summarized in Fig. 6(f). It is reasonable to deduce that δ_{CT} and δ/η may have the same origin for their similar polarization and k_z dependencies (see Figs. 4 and 5). On the other hand, α_{CT} and β_{CT} probably originate from a strong mixing of α and β during the remarkable electronic structure reconstruction, so that they appear in both s and p geometries.

C. Temperature dependence

The detailed temperature dependencies of photoemission data are shown in Fig. 7. The data collected in a sample cooling

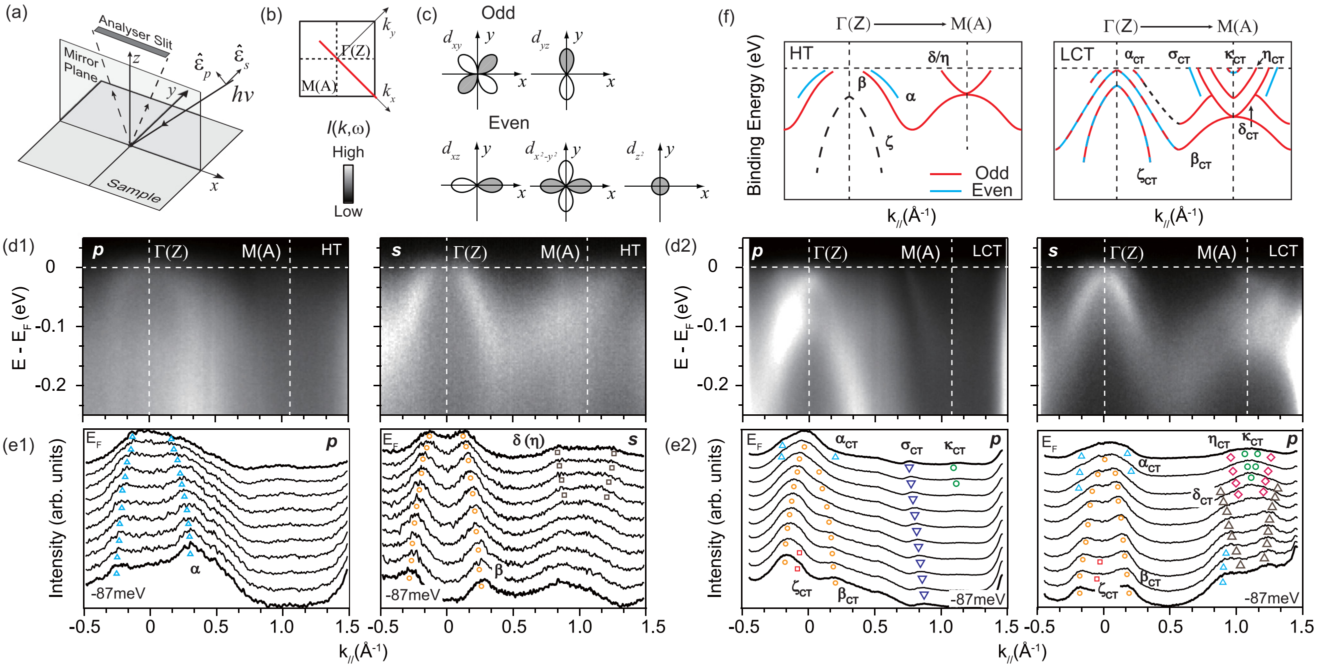

FIG. 6. (Color online) Polarization dependence of photoemission data of $\mathrm{Ca}_{1-x}\mathrm{Pr}_x\mathrm{Fe}_2\mathrm{As}_2$. (a) Experimental setup for polarization-dependent ARPES. The x and y directions are defined to be along the nearest Fe-Fe bonds. (b) Indication of cut direction in the projected two-dimensional Brillouin zone. The Γ-M direction is parallel to the k_x (k_y) direction in the reciprocal space. (c) Illustration of the spatial symmetry of the 3d orbitals with respect to the mirror plane. (d1) The photoemission intensity plots taken with 103 eV linearly polarized photons along the $\Gamma(Z)$-$M(A)$ direction in the HT phase at 90 K. The left one was taken under the p geometry, while the right one was taken under the s geometry. (e1) The corresponding MDCs for the data in panel (d1). (d2), (e2) The corresponding CT phase ($T = 16$ K) data for data in panels (d1) and (e1), respectively. Data were taken with 72 eV linearly polarized photons. (f) The summary of the orbitals (even or odd) of low-energy electronic structure in these two phases. Bands that could not be clearly resolved are represented by dashed black lines.

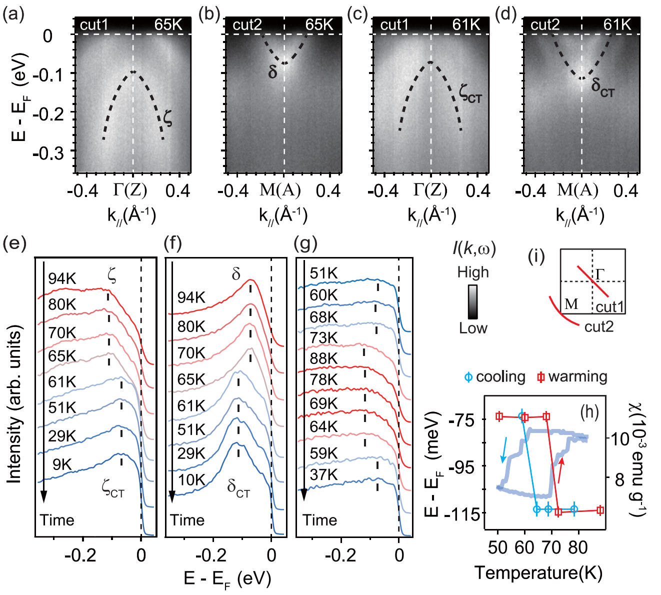

FIG. 7. (Color online) Temperature dependence of photoemission data. (a), (b) Photoemission intensity plots of $Ca_{1-x}Pr_xFe_2As_2$ measured along cuts 1 and 2, respectively, in the HT phase. (c), (d) The same for those in the CT phase as in panels (a) and (b). Dashed lines are a guide for the eyes for band dispersions. (e), (f) The EDCs at $\Gamma(Z)$ and $M(A)$ for a cooling procedure, respectively. Peak positions are indicated by short bars. (g) The EDCs of $Ca_{1-x}Pr_xFe_2As_2$ at the zone center [$\Gamma(Z)$] for a warming-cooling cycle. (h) The summary of band tops of ζ (ζ_{CT}) obtained in panel (g), which exhibits a hysteresis. The dc susceptibility in Fig. 1(d) is overlaid for comparison (translucent blue lines). (i) Indication of cut directions in the projected two-dimensional Brillouin zone. All data were taken with randomly polarized 21.2 eV photons.

procedure are presented in Figs. 7(a)–7(f). The representative photoemission intensity plots along cuts 1 and 2 [illustrated in Fig. 7(i)] are shown in Figs. 7(a) and 7(b) for the HT phase, while those for the CT phase are presented in Figs. 7(c) and 7(d). The corresponding EDCs at the $\Gamma(Z)$ and $M(A)$ points are stacked in Figs. 7(e) and 7(f), respectively. The peak positions of ζ (ζ_{CT}) and δ (δ_{CT}) change discontinuously across the CT transition, indicating that the reconstruction occurs abruptly. By applying parabolic fitting, the energy shift for the band tops of α and β are estimated to be 5 meV (from 15 to 10 meV) and −27 meV (from 10 to −17 meV) upon cooling, respectively.

Since the magnetic susceptibility shows a hysteresis loop, it is intriguing to investigate whether a similar hysteresis could be observed for the electronic structure. The EDCs at the zone center taken in a warming-cooling cycle are stacked in Fig. 7(g). The temperature dependence of the band top of the ζ (ζ_{CT}) band is summarized in Fig. 7(h). The clear hysteresis in the electronic structure reconstruction is qualitatively consistent with the bulk transport properties, including the temperature dependence of the Hall coefficient [15]. This suggests the measured electronic structure somewhat reflects the bulk properties and the reconstruction is directly linked with the CT transition. Little deviation in the transition temperature is likely due to some sample variations.

IV. DISCUSSION AND CONCLUSION

Previous theoretical works suggest that the remarkable change in the crystal structure across the CT transition, associated with the formation of As-As bonding [9,10,35], quenches the magnetic moments of Fe and leads to the electronic structure reconstruction in the CT phase of $Ca_{1-x}Pr_xFe_2As_2$. However, compared with those of $Ca(Fe_{1-x}Rh_x)_2As_2$ and the annealed $CaFe_2As_2$, the reconstruction across CT transition in $Ca_{1-x}Pr_xFe_2As_2$ is rather different. In $Ca(Fe_{1-x}Rh_x)_2As_2$ and the annealed $CaFe_2As_2$, the vanishment of the hole cylindrical Fermi surface was argued to be intimately linked with the absence of superconductivity in the CT phase. However, the hole pocket persists in the CT phase of $Ca_{1-x}Pr_xFe_2As_2$, which is intrinsically nonsuperconducting, and the nesting condition still holds. This finding indicates that the absence of magnetic ordering and superconductivity in the CT phase is not necessarily correlated with the presence or absence of a hole pocket.

Around the zone corner, four bands (κ_{CT}, η_{CT}, δ_{CT}, and σ_{CT}) are found in the CT phase of $Ca_{1-x}Pr_xFe_2As_2$, while only one electronlike band is found in the CT phase of $Ca(Fe_{1-x}Rh_x)_2As_2$ and the annealed $CaFe_2As_2$. One possibility is that some of these bands might have a surface origin. However, the observed 1 × 2 and 2 × 1 surface reconstructions should contribute to the band folding at the X point rather than the M point [29,30], thus they are unlikely due to surface states. They are also unlikely to be caused by the weak magnetic ordering of praseodymium dopants at low temperatures [23], since it was shown before that the ordering of Eu moment in $EuFe_2As_2$ does not cause a noticeable change to its low-energy electronic structure [36]. Therefore, the unique band structure of $Ca_{1-x}Pr_xFe_2As_2$ is likely intrinsic, but further band structure calculations are needed to investigate how these additional bands are caused by the CT structural transition.

Our data show that almost all the bands tend to be more dispersive in the CT phase than in the HT phase of $Ca_{1-x}Pr_xFe_2As_2$. We applied parabolic-curve fittings to evaluate the effective mass of each band in these two phases in approximately the same k_z plane. The effective mass of δ in the HT phase slightly reduces from $1.73 \pm 0.02m_e$ to $1.6 \pm 0.1m_e$ (δ_{CT}) in the CT phase. More evidently, the absolute values of the effective mass of α and β are $10.0 \pm 0.4m_e$ and $4.1 \pm 0.5m_e$, respectively, while in the CT phase, those values of α_{CT} and β_{CT} are $5.7 \pm 0.1m_e$ and $2.0 \pm 0.1m_e$, respectively. The reduction of effective mass indicates the suppression of electronic correlations in the CT phase, which is also the case in $CaFe_2As_2$ [17,37–39]. For iron-based superconductors, it was proposed in the strong-coupling pairing scenario that the superconducting pairing is mediated by the local antiferromagnetic exchange interaction [40], which is linked to the reasonably strong electronic correlations or narrow bandwidth [26]. Since the Fermi surface topology might be less relevant, it may be more likely that the weakened correlations in the CT phase suppress the magnetic fluctuation, and subsequently push the system into the nonsuperconducting regime [26].

In summary, we report detailed ARPES results on $Ca_{1-x}Pr_xFe_2As_2$ single crystals. Across the CT transition, the sizable change in the crystal structure leads to the drastic electronic structure reconstruction. Our results show discrepancies with the band calculations of $CaFe_2As_2$ and significant mixing of different orbitals in the CT phase, which still call for further theoretical investigations. Instead of the lack of Fermi surface nesting between electron and hole Fermi surfaces, we propose that the weakening of electronic correlations might be responsible for the absence of magnetic ordering and superconductivity in the CT phase.

ACKNOWLEDGMENTS

Some of the preliminary data (not shown here) were taken at APE beamline of ELETTRA synchrotron light source. We gratefully thank Ivana Vobornik at ELETTRA, D. H. Lu and Y. Zhang at SSRL, and Ming Shi at SLS for technical support. This work is supported in part by the National Science Foundation of China and National Basic Research Program of China (973 Program) under Grants No. 2012CB921402, No. 2012CB927401, No. 2011CB921802, No. 2011CBA00112, and No. 2011CBA00106. D.W.S. is also supported by the "Strategic Priority Research Program (B)" of the Chinese Academy of Sciences (Grant No. XDB04040300). SSRL is operated by the US DOE Office of Basic Energy Science.

---

[1] C. de la Cruz, Q. Huang, J. W. Lynn, J. Li, W. Ratcliff, II, J. L. Zarestky, H. A. Mook, G. F. Chen, J. L. Luo, N. L. Wang, and P. Dai, Nature (London) **453**, 899 (2008).

[2] M. Rotter, M. Tegel, D. Johrendt, I. Schellenberg, W. Hermes, and R. Pöttgen, Phys. Rev. B **78**, 020503(R) (2008).

[3] X. H. Chen, T. Wu, G. Wu, R. H. Liu, H. Chen, and D. F. Fang, Nature (London) **453**, 761 (2008).

[4] M. Rotter, M. Tegel, and D. Johrendt, Phys. Rev. Lett. **101**, 107006 (2008).

[5] K. Sasmal, B. Lv, B. Lorenz, A. M. Guloy, F. Chen, Y.-Y. Xue, and C.-W. Chu, Phys. Rev. Lett. **101**, 107007 (2008).

[6] A. Kreyssig, M. A. Green, Y. Lee, G. D. Samolyuk, P. Zajdel, J. W. Lynn, S. L. Bud'ko, M. S. Torikachvili, N. Ni, S. Nandi, J. B. Leão, S. J. Poulton, D. N. Argyriou, B. N. Harmon, R. J. McQueeney, P. C. Canfield, and A. I. Goldman, Phys. Rev. B **78**, 184517 (2008).

[7] M. S. Torikachvili, S. L. Bud'ko, N. Ni, and P. C. Canfield, Phys. Rev. Lett. **101**, 057006 (2008).

[8] D. K. Pratt, Y. Zhao, S. A. J. Kimber, A. Hiess, D. N. Argyriou, C. Broholm, A. Kreyssig, S. Nandi, S. L. Bud'ko, N. Ni, P. C. Canfield, R. J. McQueeney, and A. I. Goldman, Phys. Rev. B **79**, 060510 (2009).

[9] T. Yildirim, Phys. Rev. Lett. **102**, 037003 (2009).

[10] W. Ji, X.-W. Yan, and Z.-Y. Lu, Phys. Rev. B **83**, 132504 (2011).

[11] J. H. Soh, G. S. Tucker, D. K. Pratt, D. L. Abernathy, M. B. Stone, S. Ran, S. L. Bud'ko, P. C. Canfield, A. Kreyssig, R. J. McQueeney, and A. I. Goldman, Phys. Rev. Lett. **111**, 227002 (2013).

[12] H. Gretarsson, S. R. Saha, T. Drye, J. Paglione, J. Kim, D. Casa, T. Gog, W. Wu, S. R. Julian, and Y.-J. Kim, Phys. Rev. Lett. **110**, 047003 (2013).

[13] A. I. Coldea, C. M. J. Andrew, J. G. Analytis, R. D. McDonald, A. F. Bangura, J.-H. Chu, I. R. Fisher, and A. Carrington, Phys. Rev. Lett. **103**, 026404 (2009).

[14] S. Ran, S. L. Bud'ko, D. K. Pratt, A. Kreyssig, M. G. Kim, M. J. Kramer, D. H. Ryan, W. N. Rowan-Weetaluktuk, Y. Furukawa, B. Roy, A. I. Goldman, and P. C. Canfield, Phys. Rev. B **83**, 144517 (2011).

[15] S. R. Saha, N. P. Butch, T. Drye, J. Magill, S. Ziemak, K. Kirshenbaum, P. Y. Zavalij, J. W. Lynn, and J. Paglione, Phys. Rev. B **85**, 024525 (2012).

[16] K. Tsubota, T. Wakita, H. Nagao, C. Hiramatsu, T. Ishiga, M. Sunagawa, K. Ono, H. Kumigashira, M. Danura, K. Kudo, M. Nohara, Y. Muraoka, and T. Yokoya, J. Phys. Soc. Jpn. **82**, 073705 (2013).

[17] R. S. Dhaka, R. Jiang, S. Ran, S. L. Bud'ko, P. C. Canfield, B. N. Harmon, A. Kaminski, M. Tomić, R. Valentí, and Y. Lee, Phys. Rev. B **89**, 020511(R) (2014).

[18] K. Gofryk, B. Saparov, T. Durakiewicz, A. Chikina, S. Danzenbächer, D. V. Vyalikh, M. J. Graf, and A. S. Sefat, Phys. Rev. Lett **112**, 186401 (2014).

[19] Y.-Z. Zhang, H. C. Kandpal, I. Opahle, H. O. Jeschke, and Roser Valentí, Phys. Rev. B **80**, 094530 (2009).

[20] M. Tomić, R. Valentí, and H. O. Jeschke, Phys. Rev. B **85**, 094105 (2012).

[21] B. Lv, L. Deng, M. Gooch, F. Wei, Y. Sun, J. K. Meen, Y.-Y. Xue, B. Lorentz, and C.-W. Chu, Proc. Natl. Acad. Sci. USA **108**, 15705 (2011).

[22] Y. Qi, Z. Gao, L. Wang, D. Wang, X. Zhang, C. Yao, C. L. Wang, C. D. Wang, and Y. Ma, Supercond. Sci. Technol. **25**, 045007 (2012).

[23] L. Ma, G.-F. Gi, J. Dai, S. R. Saha, T. Drye, J. Paglione, and W.-Q. Yu, Chin. Phys. B **22**, 057401 (2013).

[24] I. Zeljkovic, D. Huang, C.-L. Song, B. Lv, C.-W. Chu, and J. E. Hoffman, Phys. Rev. B **87**, 201108(R) (2013).

[25] K. Gofryk, M. Pan, C. Cantoni, B. Saparov, J. E. Mitchell, and A. S. Sefat, Phys. Rev. Lett. **112**, 047005 (2014).

[26] Z. R. Ye, Y. Zhang, F. Chen, M. Xu, J. Jiang, X. H. Niu, C. H. P. Wen, L. Y. Xing, X. C. Wang, C. Q. Jin, B. P. Xie, and D. L. Feng, Phys. Rev. X **4**, 031041 (2014).

[27] S. R. Saha, N. P. Butch, K. Kirshenbaum, J. Paglione, and P. Y. Zavalij, Phys. Rev. Lett. **103**, 037005 (2009).

[28] B. Lv, F. Y. Wei, L. Z. Deng, Y. Y. Xue, and C. W. Chu, arXiv:1308.3129.

[29] E. van Heumen, J. Vuorinen, K. Koepernik, F. Massee, Y. Huang, M. Shi, J. Klei, J. Goedkoop, M. Lindroos, J. van den Brink, and M. S. Golden, Phys. Rev. Lett. **106**, 027002 (2011).

[30] Y.-B. Huang, R. Pierre, J.-H. Wang, X.-P. Wang, X. Shi, N. Xu, Z. Wu, A. Li, J.-X. Yin, T. Qian, B. Lv, C.-W. Chu, S.-H. Pan, M. Shi, and H. Ding, Chin. Phys. Lett. **30**, 017402 (2013).

[31] C. Liu, T. Kondo, N. Ni, A. D. Palczewski, A. Bostwick, G. D. Samolyuk, R. Khasanov, M. Shi, E. Rotenberg, S. L. Bud'ko,

P. C. Canfield, and A. Kaminski, Phys. Rev. Lett. **102**, 167004 (2009).

[32] F. Chen, Y. Zhang, J. Wei, B. Zhou, L. X. Yang, F. Wu, G. Wu, X. H. Chen, and D. L. Feng, J. Phys. Chem. Solids **72**, 469 (2011).

[33] Y. Zhang, F. Chen, C. He, B. Zhou, B. P. Xie, C. Fang, W. F. Tsai, X. H. Chen, H. Hayashi, J. Jiang, H. Iwasawa, K. Shimada, H. Namatame, M. Taniguchi, J. P. Hu, and D. L. Feng, Phys. Rev. B **83**, 054510 (2011).

[34] Y. Zhang, C. He, Z. R. Ye, J. Jiang, F. Chen, M. Xu, Q. Q. Ge, B. P. Xie, J. Wei, M. Aeschlimann, X. Y. Cui, M. Shi, J. P. Hu, and D. L. Feng, Phys. Rev. B **85**, 085121 (2012).

[35] N. Colonna, G. Profeta, A. Continenza, and S. Massidda, Phys. Rev. B **83**, 094529 (2011).

[36] B. Zhou, Y. Zhang, L. X. Yang, M. Xu, C. He, F. Chen, J. F. Zhao, H. W. Ou, J. Wei, B. P. Xie, T. Wu, G. Wu, M. Arita, K. Shimada, H. Namatame, M. Taniguchi, X. H. Chen, and D. L. Feng, Phys. Rev. B **81**, 155124 (2010).

[37] Y. Furukawa, B. Roy, S. Ran, S. L. Bud'ko, and P. C. Canfield, Phys. Rev. B **89**, 121109(R) (2014).

[38] J. Diehl, S. Backes, D. Guterding, H. O. Jeschke, and Roser Valentí, Phys. Rev. B **90**, 085110 (2014).

[39] S. Mandal, R. E. Cohen, and K. Haule, Phys. Rev. B **90**, 060501(R) (2014).

[40] J. Hu and H. Ding, Sci. Rep. **2**, 381 (2012).